Journal of Neuroinflammation

RESEARCH

Open Access

Macrophage exosomal miR-30c-2-3p in atherosclerotic plaques aggravates microglial neuroinflammation during large-artery atherosclerotic stroke via TGF-β/SMAD2 pathway

Yue Tang[1,2,3†], Ming-Hao Dong[1,2,3†], Xiao-Wei Pang[1,2,3†], Hang Zhang[1,2,3], Yun-Hui Chu[1,2,3], Luo-Qi Zhou[1,2,3], Sheng Yang[1,2,3], Lu-Yang Zhang[1,2,3], Yun-Fan You[1,2,3], Li-Fang Zhu[1,2,3], Wei Wang[1,2,3], Chuan Qin[1,2,3*] and Dai-Shi Tian[1,2,3*]

Abstract

Circulating miR-30c-2-3p has been closely related to vascular diseases, however, its role and underlying mechanisms in ischemic stroke remained unclear. Our study addressed this gap by observing elevated levels of exosomal miR-30c-2-3p in patients with acute ischemic stroke due to large artery atherosclerosis. Further investigation revealed that these exosomal miR-30c-2-3p primarily originated from macrophages within atherosclerotic plaques, exacerbating ischemic stroke by targeting microglia. Exosomes enriched with miR-30c-2-3p increased microglial inflammatory properties in vivo and aggravated neuroinflammation by inhibiting SMAD2. In summary, our findings revealed a novel mechanism whereby macrophage-derived foam cells within atherosclerotic plaques secrete exosomes with high levels of miR-30c-2-3p, thus aggravate brain damage during ischemic stroke, which serves as crucial link between the periphery and brain.

Keywords Exosomes, MiR-30c-2-3p, Atherosclerosis, Microglia, Inflammation

Introduction

Large artery atherosclerosis (LAA) presents a challenge due to its high recurrence rate and limited treatment options, often resulting in severe neurological deficits [1, 2]. Despite significant investment in emergency stroke care, many patients still fail to receive timely treatment due to the narrow therapeutic window [3]. Given the complex nature of ischemic stroke with atherosclerosis [4], therapeutic strategy advancing and functional outcome salvaging remains an instant research area.

Exosomes, micro-vesicles encased in a phospholipid bilayer and ranging from 40 to 160 nm in diameter, are capable of transversing the blood–brain barrier [5], making them significant players in intercellular

†Yue Tang, Ming-Hao Dong and Xiao-Wei Pang contributed equally to this work.

*Correspondence:
Chuan Qin
chuanqin@tjh.tjmu.edu.cn
Dai-Shi Tian
tiands@tjh.tjmu.edu.cn
[1] Department of Neurology, Tongji Hospital, Tongji Medical College, Huazhong University of Science and Technology, Wuhan 430030, China
[2] Hubei Key Laboratory of Neural Injury and Functional Reconstruction, Huazhong University of Science and Technology, Wuhan 430030, China
[3] Key Laboratory of Vascular Aging, Ministry of Education, Tongji Hospital of Tongji Medical College, Huazhong University of Science and Technology, 430030 Wuhan, People's Republic of China

communication. Laden with a diverse array of biologically active substances, such as proteins, lipids, nucleic acids and metabolites, exosomes serve pivotal roles in both physiological and pathological states and their composition reflecting their cellular origin [6–8]. While extensively studied in tumor metastasis and neurological disorders like Alzheimer's, multiple sclerosis, Parkinson's, and glioma [9–11], their involvement in acute ischemic stroke (AIS) remains incompletely understood. Notably, during atherosclerosis-induced AIS, inflammatory cells, foam cells, and damaged endothelial cells release copious amounts of exosomes [12–15]. These exosomes, linked to atherosclerosis and plaque vulnerability, may facilitate cell–cell communication within plaques and beyond, potentially carrying inflammatory factors to distant vascular endothelial cells [16–20]. Additionally, it has been observed that miR-30c-2-3p is implicated in the oncogenesis of various tumors and associated with vascular-related diseases, such as pulmonary arterial hypertension, renal vascular disease, and coronary heart disease (CHD) [21–23]. Serum mir-30c-2-3p was reported to be increased in CHD compared with controls by next-generation small RNA sequencing [21]. Moreover, the expression level of mir-30c-2-3p was found to be significantly higher in plasma exosomes of Parkinson's patients than in controls [24, 25]. The above studies suggested that circulating mir-30c-2-3p could be used as a potential biomarker [26, 27]. However, little is known about its role in AIS. Hence, we propose that exosomal miR-30c-2-3p from atherosclerotic plaques could serve as vehicles conveying messages from the plaque to remote brain tissue via their cargo of bioactive molecules, representing a novel mechanism in ischemic stroke development.

In this study, we revealed that plasma exosomal miR-30c-2-3p exhibited upregulation in AIS patients. The specific elevation of exosomal miR-30c-2-3p in LAA was distinguishable from other AIS subtypes. Moreover, we illustrated that exosomes harboring miR-30c-2-3p originated from macrophages in atherosclerotic plaques through an in vivo *ApoE*$^{-/-}$ atherosclerotic mouse model and bone marrow-derived macrophages (BMDM)-induced foam cells in vitro. The exosomal miR-30c-2-3p was internalized by microglia/macrophages in ischemic lesions, promoting a pro-inflammatory property. This process was associated with downregulation of SMAD2, an anti-inflammatory factor within the TGF-β signaling pathway. These findings established a bridge between atherosclerotic plaque and the brain via circulating exosomal miR-30c-2-3p, proposing a novel mechanism contributing to the exacerbation of ischemic stroke due to LAA.

Material and methods

Patient samples and clinical characteristics

One hundred-four patients were included from September 1, 2020 to August 31, 2022. The study was approved by the Ethics Committee of Tongji Hospital (S065) and eligible subjects gave informed signed consent. All enrolled patients with AIS were diagnosed by two neurologists and assessed to classify their TOAST types as large artery atherosclerosis (LAA), cardioembolic (CE) or small vessel occlusion (SVO). Controls were defined as healthy individuals included from physical examination center. Supplementary Table 1 summarizes the demographic and clinical characteristics of the entire cohort.

Blood samples were collected into EDTA anticoagulation tubes (BD Vacutainer, 3678636). Then blood was left at room temperature for 2 h and processed immediately at 4 °C, spun at 1500*g* for 10 min, plasma was stored at − 80 °C refrigerator for subsequent experimental detection.

Carotid endarterectomy samples

In this study, a total of 30 human carotid endarterectomy tissues were collected and semi-quantitatively classified as stable or unstable plaque according to their histological features as described in the literature [28, 29]. The demographic and clinical characteristics of this cohort was showed in Supplementary Table 2. The samples were perfused with saline, fixed with 4% PFA for 24 h, then immersed in 30% sucrose solutions for 48 h, embedded in OCT, and sectioned at 7-μM thickness.

For the staining of frozen sections, tissue slides were washed with PBS for 5 min, followed by staining with haematoxylin and eosin (H&E, Solarbio, G1120), and Masson's trichrome (Solarbio, G1120) according to the manufacture's instruction. After washing, slides were mounted with Neutral balsam (Solarbio, 96949-21-2).

For RNA-FISH and immunofluorescence co-staining, Cy3-labbled miR-30c-2-3p probe (5′–3′ GUGC + UCU CCCGC + UGAGCUA) was co-stained with CD68 (R&D, MAB20401, 1:200), and αSMA (Sigma, A2547, 1:200) in human atherosclerotic plaques to validate expression of miR-30c-2-3p in. Using BersinBioTM Immunofluorescence-Fluorescent in situ hybridization (IF-FISH) Kit (Bes1023, BersinBio), plaque slices were pretreated, prehybridized, hybridized and washed followed by immunostaining, according to manufacturer's instructions.

Experimental animals

A total of 200 male B6/JGpt-Apoe^{em1Cd82}/Gpt (*ApoE*$^{-/-}$) mice (provided by GemPharmatech Co. Ltd., Nanjing, China) were used. Adult and neonatal C57BL/6J mice were obtained from Vital River Laboratory Animal

Technology Co. Ltd., Beijing, China. All animals were housed in specific-pathogen-free condition and studies were approved by the Institutional Review Board of Tongji Hospital (TJ-IRB20201022). Eight-week $ApoE^{-/-}$ mice were given for twelve weeks high-fat diet containing 41% fat (41 kcal% fat, 0.21% cholesterol, 4686 kcal/kg) purchased from Research Diets (D12079B, USA) to induce atherosclerosis model, as previously described. Meanwhile, eight-week $ApoE^{-/-}$ mice were given normal diet for 12 weeks as controls.

Murine samples collection

At the age of 20 weeks, mice were anesthetized, with blood samples were collected and centrifuged at 1000*g* for 10 min at 4 ℃. After blood collection, 2 mL of 5 mM EDTA solution was instilled, followed by 20 mL of sterile PBS. Then the plaque tissues were stripped including from the bifurcation of the carotid artery to the common iliac artery and placed in sterile PBS. After all plaques isolated, they were placed in 1640 RPMI medium, and the arterial tissues from three mice were defined as one sample for analysis. Subsequently, the tissues were carefully cut into 1 mm^3 pieces in a biosafety cabinet. After digestion and dissociation with 120 U/mL DNase I, 120 U/mL hyaluronidase, 250 U/mL collagenase XI, 450 U/mL collagenase I, the digests were passed through 70 μm and 40 μm filters, and spun at 600 g for 10 min at 25 ℃ and then centrifuged at 2000*g* for 20 min at 4 ℃, finally the supernatant was stored at − 80 ℃.

Additionally, some carotid artery and aorta were immediately photographed with Nikon or fixed in 4% paraformaldehyde at 4 ℃ for 24 h, and replaced with 30% sucrose solution to dehydrate for 48 h, then OCT-embedded sections were sliced at a thickness of 7 μm.

Transient focal cerebral ischemia surgery and exosomes injection

Transient Middle Cerebral Artery Occlusion operation as described as previous study [30], was established by a nylon suture causing intraluminal occlusion of the right middle cerebral artery for 1 h. Briefly, mice were anesthetized by inhalation of isoflurane, and the right common and internal carotid artery were exposed and ligated temporarily. A nylon suture coated with silicon was gently inserted into the external carotid artery, then advanced carefully into farther internal carotid artery and the circle of Willis. The efficacy of occlusion was monitored by Laser Doppler flow cytometry showed an 80% or more cerebral blood flow reduction. The nylon suture was removed to re-perfuse after one hour occluding.

Exosomes or PKH26-labeled exosomes isolated from plasma of $ApoE^{-/-}$ mice fed with high fat or normal diet were injected into MCAO mice through tail intravenous (150 μg, dissolved in normal saline at a final concentration of 0.75 μg/μL) once a day for three consecutive days from the day of surgery, as the previous study [31] described with little modification.

Exosomes labelling

The extracted plasma exosome suspension was diluted to 500 μL with reagent Diluent C from the PKH26 kit (Sigma-Aldrich, MINI26); 4 μL of PKH26 stain was added, blown and mixed, and incubated for 4 min at room temperature and protected from light; excess dye was closed with 4 mL of 5% BSA solution, subsequently diluted with a large amount of PBS suitable for ultracentrifugation tubes. After centrifugation, the supernatant was discarded and the red precipitate was resuspended in 500 μL PBS.

Nissl staining

Nissl staining was performed to assess the infarct area as previously described [32] with some modification. Briefly, frozen sections were demyelinated through grade alcohol (75%, 95% and 100% alcohol) for 3 min, respectively, and rinsed in distilled water for 2 min. Subsequently, the sections were stained with 0.1% toluidine blue solution for 10 min at room temperature, then quickly rinsed in distilled water and differentiated in 95% ethyl alcohol until obvious infarct border appeared. The infarct area (%) indicated the proportion of the infarct area to the area of total brain. Six inconsecutive sections with 100 μm interval of one sample were calculated.

Oil Red O staining

Fresh Oil Red O (ORO, Solarbio, G1260, 60%) staining working solution was prepared according to the manufactures' instruction at room temperature within 10 min. The sections were washed with PBS and then distilled water for 5 min, and were immersed in 60% isopropanol for 30 s. The staining working solution was dropped on the tissue sections to cover completely, stained for 2–3 min at room temperature and protected from light. 60% isopropanol was quickly used to wash the background staining off, followed by rinsing the floating dye under tap water. Then the sections were air-dried and sealed with 50% glycerol, stored at 4 ℃ for timely microscopic observation and photographic preservation.

Exosomes isolation

The plasma of human or mice from − 80 °C refrigerator was thaw in a 25 °C water bath and diluted with equal volume of PBS. The mixture was then centrifuged at 2000*g* for 10 min, the supernatant was transferred to another clean tube and spun at 12,000*g* for 20 min, followed by passing through a 0.22 μm filter to transfer the

supernatant to an ultracentrifuge tube. Then the liquid was ultracentrifuged (Beckman Coulter Optima Man-XP ultracentrifuge, TLA 120.2 rotor) at 160,000*g* for 60 min at 4 °C, the supernatant was discarded and the pellets were resuspended with 50 μL PBS, aliquoted and stored at − 80 °C or used immediately for experiments.

The digestion was thaw in a 25 °C water bath and transferred into high-speed centrifuge tube, spun at 16,000*g* for 35 min at 4 °C, followed by filtering through a 0.22 μm filter to transfer to a 26.1 mL ultracentrifuge tube spinning at 160,000*g* for 90 min at 4 °C (Beckman Coulter Optima XPN-100 ultracentrifuge, 70Ti). The supernatant was discarded and exosome pellets were resuspended in 100 μL PBS, aliquoted and stored at − 80 °C or used immediately for experiments.

The cell medium of bone marrow derived macrophage (BMDM) was collected and centrifuged at 600*g* for 10 min at room temperature, the supernatant was transferred to another tube, followed by centrifuging at 2000*g* for 20 min at 4 ℃, 16,000*g* for 35 min at 4 °C and 160,000*g* for 90 min at 4 °C (Beckman Coulter Optima XPN-100 ultracentrifuge, 70Ti). The pellets were resuspended in 100 μL PBS, aliquoted and stored at − 80 °C or used immediately for experiments.

Characterization of exosomes

For identification of exosomes, transmission electron microscopy (TEM, G1102, Servicebio Technology CO., Ltd, Wuhan, China) was used to observe the morphology. The enrichment of exosomes was confirmed by western blot using antibodies HSP70, TSG101, and CD9. The nanoparticle tracking analysis (NTA) was used to detect the concentration and size distribution profile of isolated exosomes, which analyzed by ZetaView PMX 110 and the processing software ZetaView 8.04.02 SP2.

Total RNA extraction of exosomes and RT-qPCR

The total RNA of exosomes was extracted using miRNeasy Micro kit (Qiagen, No. 217084), according to the protocol of the manufacture. Total RNA from microglia extracted with TRIzol. The cDNA synthesis of the specific microRNA was performed following PrimeScript™ RT Master Mix (TAKARA, RR037A or RR036A) instructions about stem-loop primer. The reverse transcription reaction was carried out in a volume of 10 μL, containing of 2 μL buffer, 0.5 μL enzyme mix, 0.5 μL specific primer, and 500 ng RNA. Quantitative PCR was conducted using Hieff qPCR SYBR Green Master Mix (YEASEN, 11201ES03), in a real-time PCR system (CFX96, Bio-Rad) for a 20 μL reaction system. The expression of target microRNA was normalized to miR-30a-5p and analyzed for relative quantification using the $2^{-\Delta\Delta CT}$ method. Primers used is provided in Supplementary Table 3.

Immunofluorescence staining

Brain or artery sections and cell culture slips were fixed in 4% PFA for 15 min. Samples were permeabilized with PBS containing 0.25% Triton X-100 for 15 min and blocked with 5% bovine serum albumin (BSA) for 60 min at room temperature. Then they were incubated with the primary antibody anti-MAC-2 (1:200; ThermoFisher, catalog #: 14-5301-82), anti-CD31 (1:100; Theremo, catalog #: 14-0311-82), anti-MAP2 (1:200; proteintech, catalog #: 17490-1-AP), anti-GFAP (1:100; CST, catalog #: 3670S), anti-IBA1(1:200; Wako, catalog #: 019-19741), anti-INOS (1:100; Abcam, catalog #: ab178945), anti-CD206 (1:200; RD, catalog #: AF2535), anti-ARG1 (1:100, Thermo, PA5-29645), overnight at 4 ℃, followed by incubation with a mixture of fluorescent secondary antibodies for 1 h at room temperature. Artery sections and BMDM slips were further stained with BODIPY 493/503 (1:1000 from a 1 mg/mL stock solution in DMSO; Thermo Fisher, D3922) for 10 min at room temperature. All samples were covered with Antifade Mountant with DAPI (Beyotime, P0131). Images were captured with a confocal microscope (OLYMPUS, FV1200). Four or six microscope fields in the infarct border region of cerebral cortex were utilized for analysis.

Primary cell culture, foam cell formation and coculture system

BMDMs were harvested from tibia and femur of WT mice at the age of 6–8 week, as described as previous study. The bone marrow was flushed and filtered with a 100 μm cell strainer, then cells were collected, washed and resuspended at the concentration of 1×10^6/mL. BMDMs were plated in 15 cm petri dish for supernatant collection or 12 well plates for other processes. Bone marrow cells were cultured with DMEM containing 20% FBS and 12.5 ng/mL of m-CSF for 7–10 days to differentiate into macrophages. Macrophages were serum-starved for 12 h and then incubated within or without 50 μg/mL of ox-LDL in DMEM supplemented with 10% exosome-depleted FBS (ultra-centrifugating for 8 h at 180,000*g*) for 24 h. Culture medium was collected and exosomes were isolated.

Neonatal C57BL/6J mice were used for primary microglia culture as previously described [33]. Briefly, the neonatal brains were minced and digested in DMEM/F12 containing 0.125% trypsin, followed by triturating and passing through a 70-μm strainer. DMEM/F12 with 20% FBS was used to resuspend and plate the cell mixtures after spinning at 1000 rpm for 5 min at 4 °C. The culture medium was replaced by DMEM/high-glucose

containing 20% FBS 3 days later and refresh medium every 3 days for 8–10 days. Microglia were isolated and collected after shaking at 180 rpm for 1 h, then seeded into 12-well plates or 24-well plates with 80–90% confluency for 24 h before further treatment.

For coculture, BMDMs/foam cells were seeded at 90% confluency in upper chamber of 12 or 24 transwell with 0.4 μm pore, while microglia pretreated with 4 h OGD in lower chamber as previously reported [34]. The levels of inflammatory-related cytokines between primary microglial cells and those with OGD/R treatment were assayed using RT-qPCR (Supplemental Fig. 2). After re-oxygenation, microglia were cocultured with BMDMs or foam cells treated with GW4869 to inhibit the secretion of macrophage-derived exosomes for 24 h.

Flow cytometry

Cells were digested with 0.25% trypsin for 3 min and suspended with 100 μL FACS buffer after washing cells twice. Cells were incubated with CD16/32 (Biolegend, 101302, 1:100) for 15 min followed by washing, then incubated with CD11b-PE/Cyanine7 (Biolegend, 101216, 1:100) and F4/80-APC (Biolegend, 123116, 1:100) for 30 min protecting from light. After washing and suspending in FACS buffer, cells were detected by Attune NxT flow cytometer and analyzed by FlowJo 10.8.

miR-30c-2-3p mimics, inhibitor and siRNA transfection

Microglia seeded in 12-well plates were treated with siRNA Smad2 or miR-30c-2-3p mimics, inhibitor and their NCs using the lipofectamine™ 3000 reagent (Thermo Fisher Scientific, L3000150). The RNAs were mixed with lipo3000 reagent and incubated 20 min at room temperature. Then the mixtures were added to cell media. After 24 h, these media were changed into PBS for 4 h OGD followed by re-oxygenation for another 24 h.

Dual luciferase assay

HEK-293T cells were seeded on 96-well plates and the transfection experiment was conducted at 80% confluence. Cells were co-transfected with psiCHECK™-2-SMAD2-UTR-WT or psiCHECK™-2-SMAD2-UTR-MUT vector and mimics NC or miR-30c-2-3p mimics for 48 h using the Lipofectamine™ 3000 Transfection Reagent following the manufacturer's instructions. Then cells were collected to perform luciferase reporter assay using the Dual-Luciferase Reporter Assay Kit (Promega Corporation, Wisconsin, USA, catalog #: E1960). The renilla luciferase activity was used to normalize the luciferase activity. Fold change of the miR-30c-2-3p mimics was calculated relative to mimics NC.

Western blotting

Cells or exosomes were lysed in ice-cold RIPA buffer (Beyotime, China) supplemented with protease inhibitor cocktail and PMSF. Proteins (30 μg) were separated by 10% SDS-PAGE and transferred onto nitrocellulose (NC) filter membranes (Boster, China) for immunoblot analysis. The membranes were blocked with 5% skimmed milk in TBST and incubated overnight at 4 ℃ with primary antibodies anti-HSP70 (1:1000, Abcam, ab181606), anti-TSG101 (1:1000, Abcam, ab125011), anti-CD9 (1:1000, Abcam, ab92726), anti-SMAD2 (1:1000, proteintech, 12570-1-AP), anti-phosphor-SMAD2 (1:1000, Abcam, ab280888; 1:1000, Abclonal, AP1342), followed by goat anti-mouse or anti-rabbit secondary antibodies incubation for 1 h at room temperature. The enhanced chemiluminescence system was used to visualize proteins expression.

Statistical analysis

Data were presented as median ± interquartile range (IQR) or mean ± standard error of the mean (SEM). Significance was assessed with Mann–Whitney U test for non-normally distributed data or Student's t-test (two-tailed) for comparisons in two groups. One-Way ANOVA analysis with post hoc Bonferroni test was performed for the normal distributed data with homogeneity of variance by GraphPad Prism software version 9. P value < 0.05 was considered statistically significant.

Results

Plasma exosomes from LAA patients exhibited elevated level of miR-30c-2-3p

A cohort of 76 AIS patients, along with 28 controls from 1 September 2020 to 31 August 2022 were enrolled in this study, 17 patients in the SVO group, 11 in the CE group and 48 in the LAA group (Fig. 1A). Exosomes were isolated from plasma using the differential-ultracentrifugation way and identified by three internationally accepted classical exosome identification methods. Transmission electron microscope (TEM) revealed the presence of spherical vesicles, consistent with the size and morphology of exosomes (Fig. 1A). Western blotting analysis demonstrated exosomal protein markers CD9, TSG101, HSP70 (Fig. 1A), and nanoparticle tracking analysis (NTA) displayed a particle diameter size distribution profile at the peak of 122.5 nm (Fig. 1A). The three dimension of exosome appearance, protein markers and diameter distribution validated that the exosomes were extracted from plasma.

To detect the expression level of plasma exosomal miR-30c-2-3p in AIS patients and controls, the stem-loop reverse transcription primers and RT-qPCR were

employed to quantify expression level of miR-30c-2-3p. Statistical analysis of $-\Delta Ct$ calculation showed that miR-30c-2-3p expression level was markedly upregulated in the LAA group after adjustment for age and sex, respectively compared to controls ($P<0.0001$), SVO group ($P=0.0005$), CE group ($P=0.0147$) (Fig. 1B). Conversely, there was no significant difference in expression level among the SVO, CE, and control groups. The receiver operating characteristic (ROC) curves were performed to evaluated the predicative power of distinguishing LAA group from controls, SVO and CE groups. The area under the curve (AUC) was respectively 0.8973 ($P<0.0001$) with sensitivity 91.67% and specificity 64.29%, 0.8113 ($P=0.0001$) with sensitivity 77.08% and specificity 64.71%, 0.6970 ($P=0.0430$) with sensitivity 60.42% and specificity 63.64% (Fig. 1C). These findings suggested that exosomal miR-30c-2-3p hold promise for identifying LAA type of AIS.

MiR-30c-2-3p was specifically expressed in macrophages within human atherosclerotic plaques

Based on the elevated level of miR-30c-2-3p in plasma exosomes of LAA patients, we hypothesized that exosomal miR-30c-2-3p may orginate from atherosclerotic plaques. According to Lovett's gold-standard semi-quantitative classification, plaques were categorized into stable and unstable type. Images analysis depicted plaques stained with H&E and Masson's Trichrome, revealing the complexity of unstable plaques, characterized by thrombus formation or extensive necrosis. Subsequently, we assessed plasma exosomal miR-30c-2-3p expression of patients with stable or unstable plaques. Interestingly, miR-30c-2-3p expression level was higher in the unstable group compared to the stable group (Fig. 1E). Patients with unstable plaques or plaque vulnerability are often associated with adverse cerebrovascular event. The ROC curve showed the expression level of miR-30c-2-3p could moderately distinguish the plaque stability (Fig. 1F). To further ascertain the correlation between miR-30c-2-3p and plaque, we quantified the percentage of different cell types with miR-30c-2-3p$^+$ puncta using miRNA-FISH combined with immunostaining, revealing that CD68$^+$ cells exhibited high expression level of miR-30c-2-3p, whereas few smooth muscle cells or other cells with plaques expressed it ($P=0.0005$). Moreover, unstable plaques displayed a higher number of miR-30c-2-3p$^+$ CD68$^+$ cells (Fig. 1G, H).

The miR-30c-2-3p level was elevated in exosomes from plasma and plaque tissues of AS mice

To further validate that plasma exosomal miR-30c-2-3p derived from atherosclerotic plaques, we utilized 7-week-old *ApoE*$^{-/-}$ mice fed a high-fat diet to induce an atherosclerosis (AS) model, while mice on a normal diet served as controls (Fig. 2A). As depicted in Fig. 2B, yellowish-white plaque tissues were visibly evident in the carotid arteries of high-fat diet-fed *ApoE*$^{-/-}$ mice. Histological analyses using H&E and ORO staining revealed a thickened intima in the aortic roots with abundant foam cells filling the subintima and a visible necrotic core. Immunofluorescence staining further illustrated extensive accumulation of lipid droplets beneath the intima, along with macrophages infiltration and foam cells engulfing lipid droplets. Subsequently, exosomes from plasma and plaque tissue digestion eluate were extracted separately and identified characters by TEM, western blot, and NTA (Fig. 2C–E). In addition, the morphology and diameter distribution of exosomes from different sources were slightly different.

The expression level of exosomal miR-30c-2-3p in plasma and plaque tissue was detected. The results showed that plasma exosomal miR-30c-2-3p in the HFD group approximately four times higher than those in the ND group, consistent with our observations in the patients' cohort, suggesting that plasma exosomes from atherosclerotic mice similarly exhibited elevated miR-30c-2-3p expression (Fig. 2F). Furthermore, exosomal miR-30c-2-3p was significantly elevated in plaque tissues, 12-fold higher than in the ND group (Fig. 2G). Furthermore, the correlation analysis of miR-30c-2-3p expression between plasma and tissue samples displayed a significant positive correlation (Fig. 2H).

(See figure on next page.)

Fig. 1 The expression of miR-30c-2-3p in human plasma exosomes and cells of atherosclerotic plaques. **A** Schematic depicting research cohorts and exosomes extraction strategy. Representative image of plasma exosomes at transmission electron microscope. Western blot analysis of plasma exosomal protein markers (HSP70, TSG101, CD9). Diameter distribution of plasma exosomes detecting by NTA (Nano tracking analysis). **B** Plasma exosomal miR-30c-2-3p level in patients with AIS categorized by TOAST criteria and controls. LAA group, n = 48; CE group, n = 11; SVO group, n = 17; Controls group, n = 28. **C** ROC curves for individual miR-30c-2-3p to separate LAA patients from controls, CE, and SVO. **D** Representative images of H&E and Masson's Trichrome staining of human atherosclerotic plaques. **E** Relative quantification of miR-30c-2-3p in patients with unstable plaque compared with stable plaque. Stable group, n = 8; Unstable group, n = 22. **F** ROC curve for individual miR-30c-2-3p to classify plaque stability. **G** Representative images of miRNA-FISH with immunostaining for CD68, White bar, 200 μm; Yellow bar, 20 μm. Percentage of CD68$^+$miR-30c-2-3p$^+$ cells in all miR-30c-2-3p$^+$ cells. **H** Representative images and relative quantification of percentage of CD68$^+$/SMA$^+$/other miR-30c-2-3p$^+$ cells in all miR-30c-2-3p$^+$ cells in patients with unstable plaque compared with stable plaque. Scale bar, 20 μm

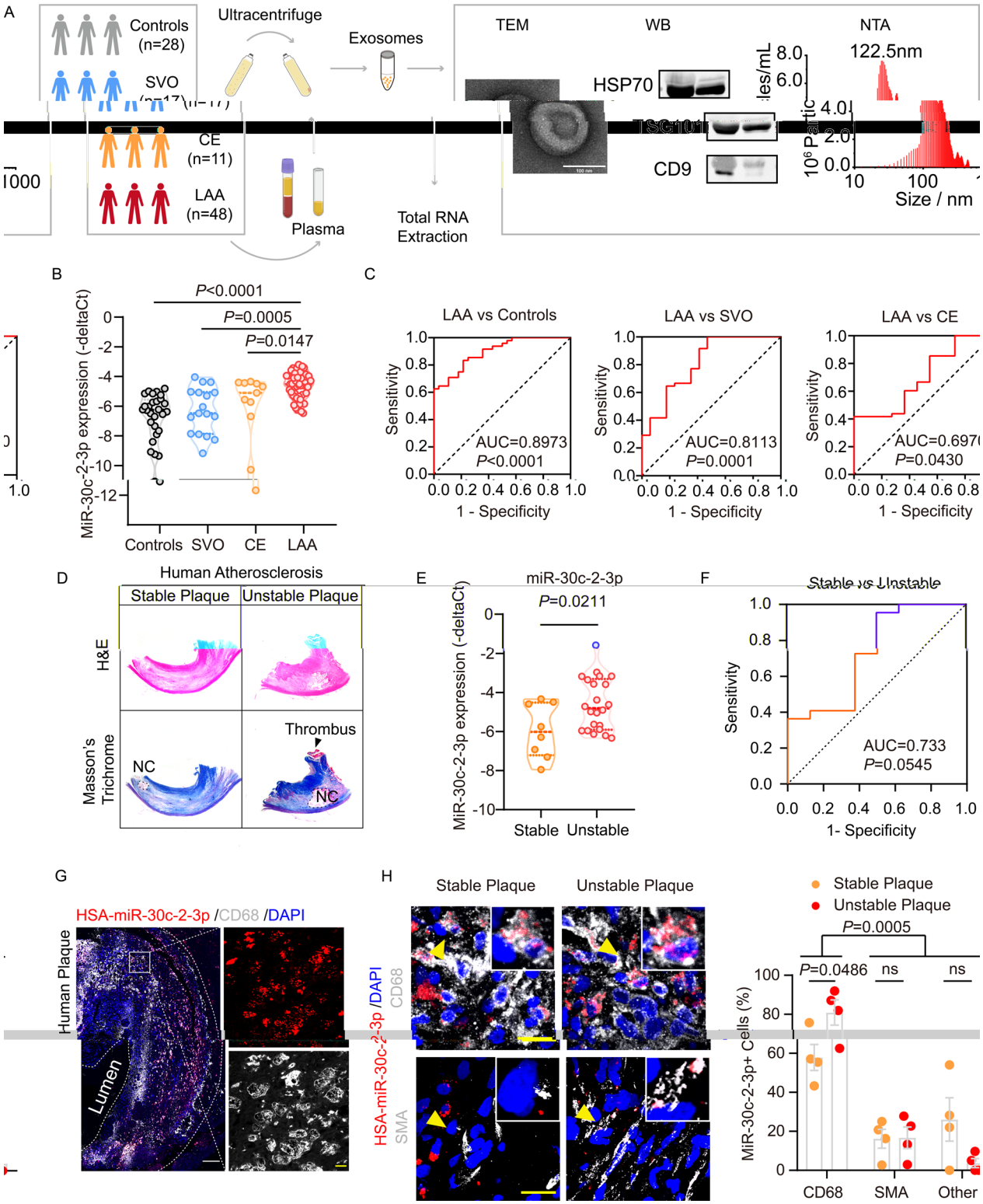

Fig. 1 (See legend on previous page.)

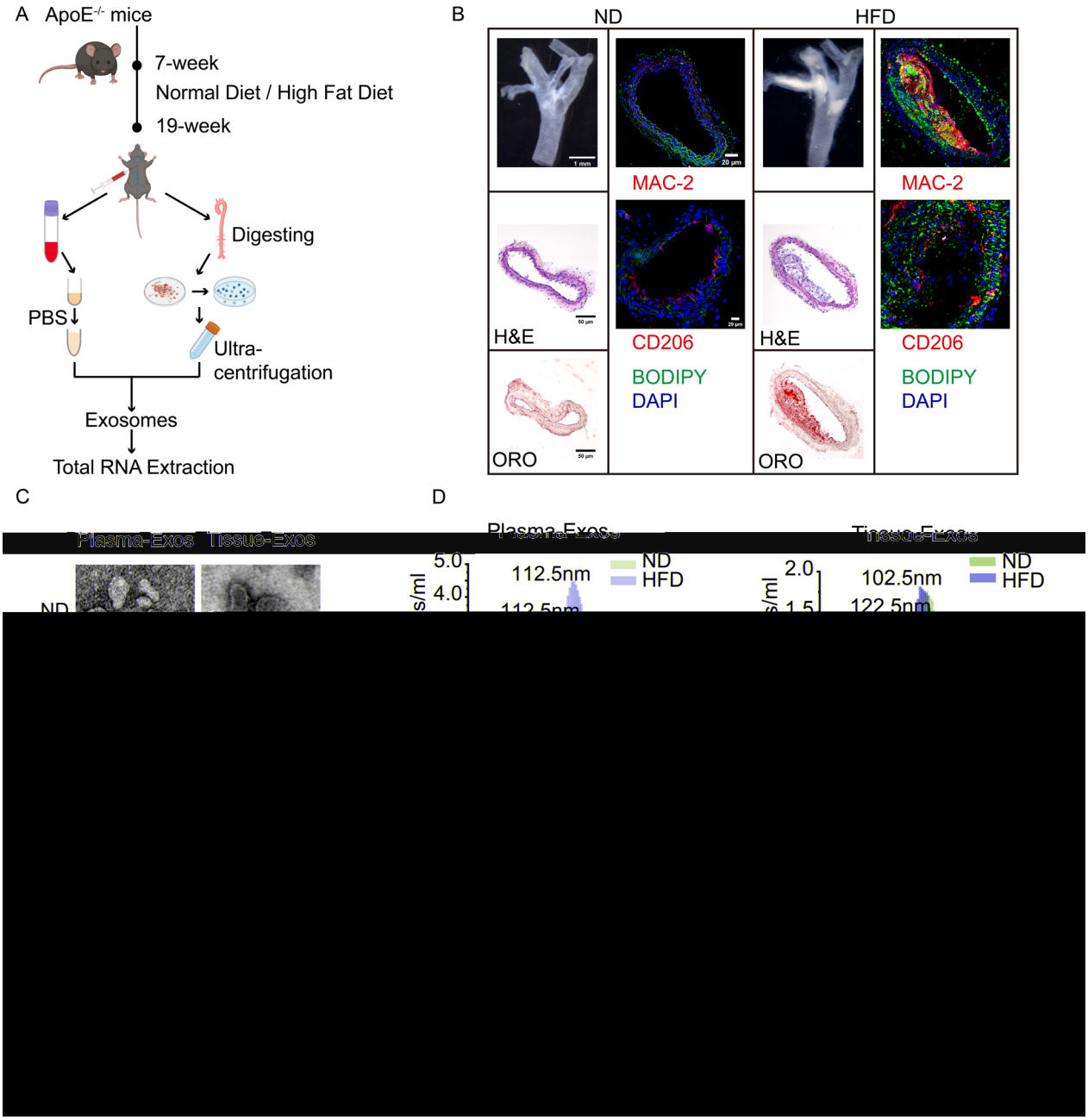

Fig. 2 The expression of exosomal miR-30c-2-3p in AS murine model. **A** Experimental schematic of AS murine model and exosomes extraction. **B** Representative images of carotid artery, Scale bar, 1 mm; aortic slices stained with H&E, ORO and immunostained by MAC-2/CD206 and Bodipy. Black scale bar, 50 μm; White scale bar, 20 μm. **C** Representative images of transmission electron microscope for mice plasma and plaque exosomes. Scale bar, 100 nm. **D** Diameter distribution of exosomes detecting by NTA. **E** Representative images of western blotting for exosomal protein markers (HSP70, TSG101, CD9). **F**, **G** Relative plasma (**F**) and plaque (**G**) exosomal miR-30c-2-3p level in HFD group increased compared with ND group (Student's t-test, two-tailed). ND group, n = 5; HFD group, n = 6

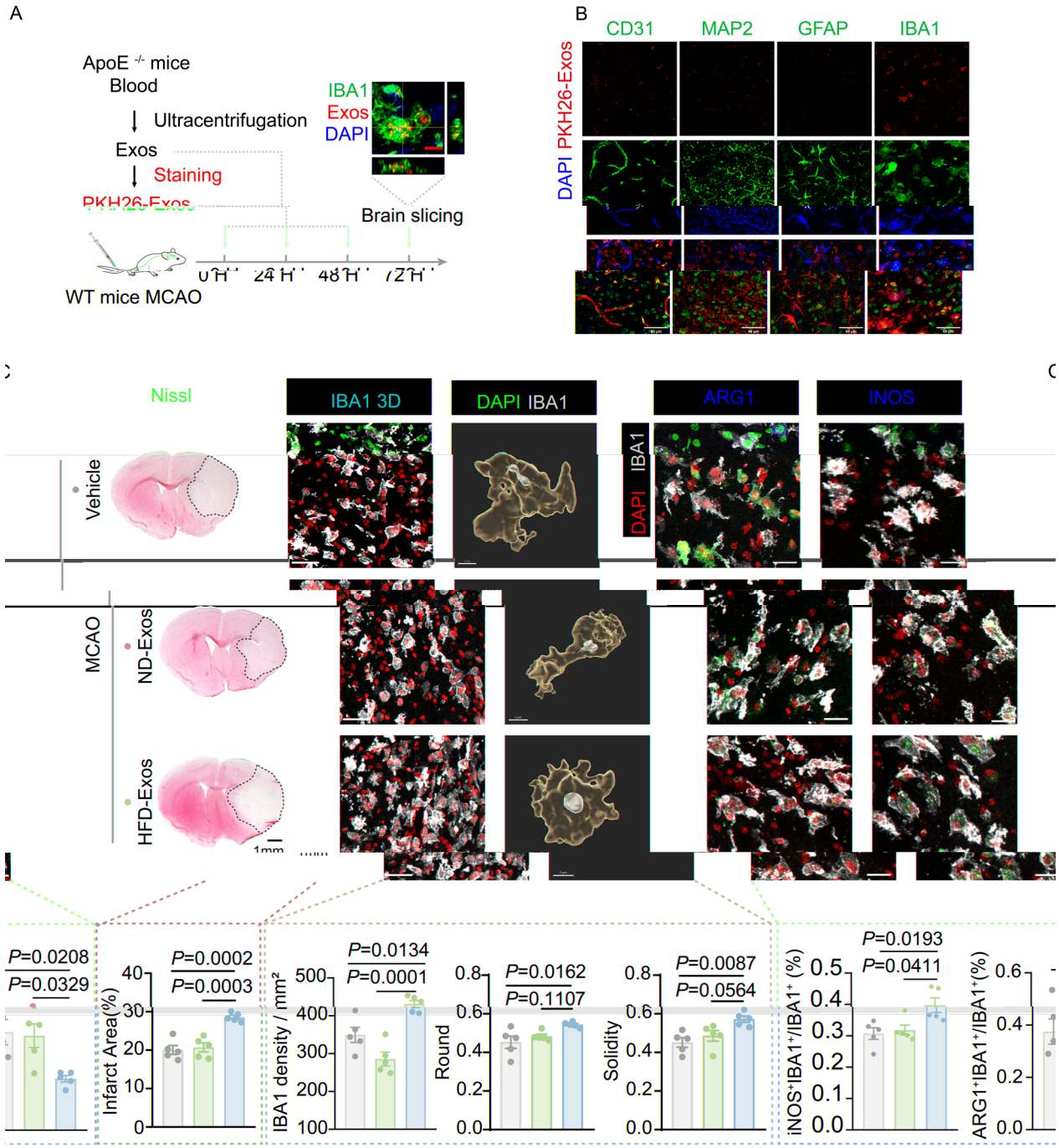

Fig. 3 Atherosclerotic plaque-derived exosomes gathered in microglia and promoted its activation and neuroinflammation in tMCAO mice. **A** MCAO conducted timeline and *AopE*$^{-/-}$ mice-derived exosomes administration; Scale bar, 10 μm. **B** Representative image of PKH26-labled exosomes colocalized with endothelia (CD31), neuron (MAP2), astrocyte (GFAP) and microglia (IBA1), respectively. Scale bar, 40 μm. **C** Representative images of Nissl staining (scale bar, 1 mm) and immunostained by IBA1 (scale bar, 40 μm) and the 3D reconstruction (scale bar, 5 μm), as well as the quantitative analysis of Iba-1^{+} cells. HFD-Exos administration regulated the pro-inflammatory phenotype of microglia with the increased iNOS expression and decreased ARG1 expression presented by immunostaining. scale bar, 20 μm; 6 image fields of each mouse were calculated as average; each group, n = 5

These results provide compelling evidence that plasma exosomes with high miR-30c-2-3p expression likely originate from atherosclerotic plaque tissues.

The plasma exosomal miR-30c-2-3p exacerbated microglial activation and neuroinflammation during ischemic stroke

To explore whether plasma exosomes with high miR-30c-2-3p expression could enter the brain and be internalized by certain cells. PKH26-labelled exosomes were administered via tail vein injection into MCAO mice (Fig. 3A). Three days later, immunofluorescence staining of brain tissue revealed predominant localization of exosomes within microglia/macrophages at the ischemic border region (Supplement Fig. 1A), with comparatively lower uptake observed in neurons, astrocytes and endothelial cells (Fig. 3B). This suggests the transport of miR-30c-2-3p into microglia via exosomes, potentially influencing microglial function.

To comprehensively elucidate the biological role of exosomes in MCAO mice, Nissl staining showed that exosomes derived from HFD resulted in a larger infarct area than ND-Exos group (Fig. 3C). Given the accumulation of exosomes in microglia, we then focused on microglial activation, through immunofluorescence staining with classic inflammatory markers. Interestingly, compared with ND-Exos, HFD-Exos caused more active microglia at the infarct border (Fig. 3C). In addition, the percentage of these active microglia co-stained with iNOS expression moderately increased, but with ARG1 expression decreased (Fig. 3C). These findings suggest that HFD-Exos derived from plasma of AS mice might aggravate infarction and promote microglial activation and neuroinflammation.

Foam cells modulated microglial activation and neuroinflammation through exosomal miR-30c-2-3p

The in vivo results suggested that exosomes with high level of miR-30c-2-3p were predominantly derived from macrophages. To validate this hypothesis, a cellular model of atherosclerosis was constructed by culturing bone marrow-derived macrophages (Fig. 4A) and subsequently given ox-LDL treatment to form foam cells. Flow cytometry analysis of BMDMs revealed that over 95% of the cells were $CD11b^{+}F4/80^{+}$ macrophages (Fig. 4B). Oil Red O staining and immunofluorescence staining confirmed the successful generation of foam cells, showing a significant accumulation of lipid droplets in macrophages (Fig. 4C).

Subsequently, the macrophages or foam cells supernatant exosomes extracted by differential-ultracentrifugation and then detected by TEM, NTA, and western blot (Fig. 4D–F). The expression of miR-30c-2-3p, detected by RT-qPCR, was significantly higher in the ox-LDL + BMDM group compared with the BMDM group (Fig. 4G), consistent with the in vivo findings. These results suggest that exosomes rich in miR-30c-2-3p may originate from macrophage-derived foam cells within atherosclerotic plaques.

To further investigate the effect of exosomal miR-30c-2-3p on microglia, a co-culture system was constructed, with macrophages pretreated with ox-LDL or not in the upper layer and microglia pretreated with OGD in the lower layer (Fig. 4H). GW4869, an exosome inhibitor, was used to prevent exosome secretion. Microglial RNA was collected and the expression of inflammatory genes were detected by RT-qPCR. Compared with the macrophage co-culture group alone, microglia co-cultured with foam cells expressed significantly higher pro-inflammatory genes *Inos*, *Nlrp3* and *Il-1b*, while anti-inflammatory genes *Tgfb* and *Arg1* were markedly decreased. And these genes expression were partially reversed in microglia co-cultured with foam cells treated by GW4869. (Fig. 4I). These results indicated that inhibiting exosomes secretion could eliminate the pro-inflammatory effect of foam cells on microglia.

MiR-30c-2-3p regulated the inflammatory properties of microglia through targeting Smad2

MicroRNAs exert their regulatory effects by targeting the 3'UTR of mRNAs, thereby modulating gene expression post-transcriptionally. Therefore, we utilized three public databases (TargetScan, miRDB, and miRWalk) for target genes prediction and finally screened out 222 candidates of miR-30-2-3p (Fig. 5A). Further pathway enrichment analysis of these target genes showed that miR-30-2-3p might be involved in the regulation of TGF-β receptor signaling pathway (Fig. 5B), which was closely related with inflammatory response. Six potential target genes, *Skil, Il17rd, Znf451, Smad2, Nrep, Lox*, involved in TGF-β receptor signaling pathway, might participate in the regulation of microglial inflammation (Fig. 5C). *Skil* [35], *Znf451* [36], *Lox* [37] as well as *Il17rd* [38] has been reported negatively regulate TGF-β receptor pathway. *Nrep* [39] down-regulates the expression of *TGF-β1* and *TGF-β2*. While *Smad2* as a transcription factor in response to TGF-β, activates TGF-β receptor pathway and acts as protective role in fibrosis and inflammation [40]. Markedly, transfection of the miR-30c-2-3p mimics causing suppression of *Smad2* protein expression in OGD/R treated microglia (Fig. 5D). To validate whether miR-30c-2-3p targeted *Smad2* 3′UTR or not, Luciferase reporter vectors containing wild-type and mutated 3′UTR of mouse *Smad2* were constructed. The mimics of miR-30c-2-3p transfection inhibited the activity of *Smad2* 3′UTR in 293 T cells, which indicated that *Smad2*

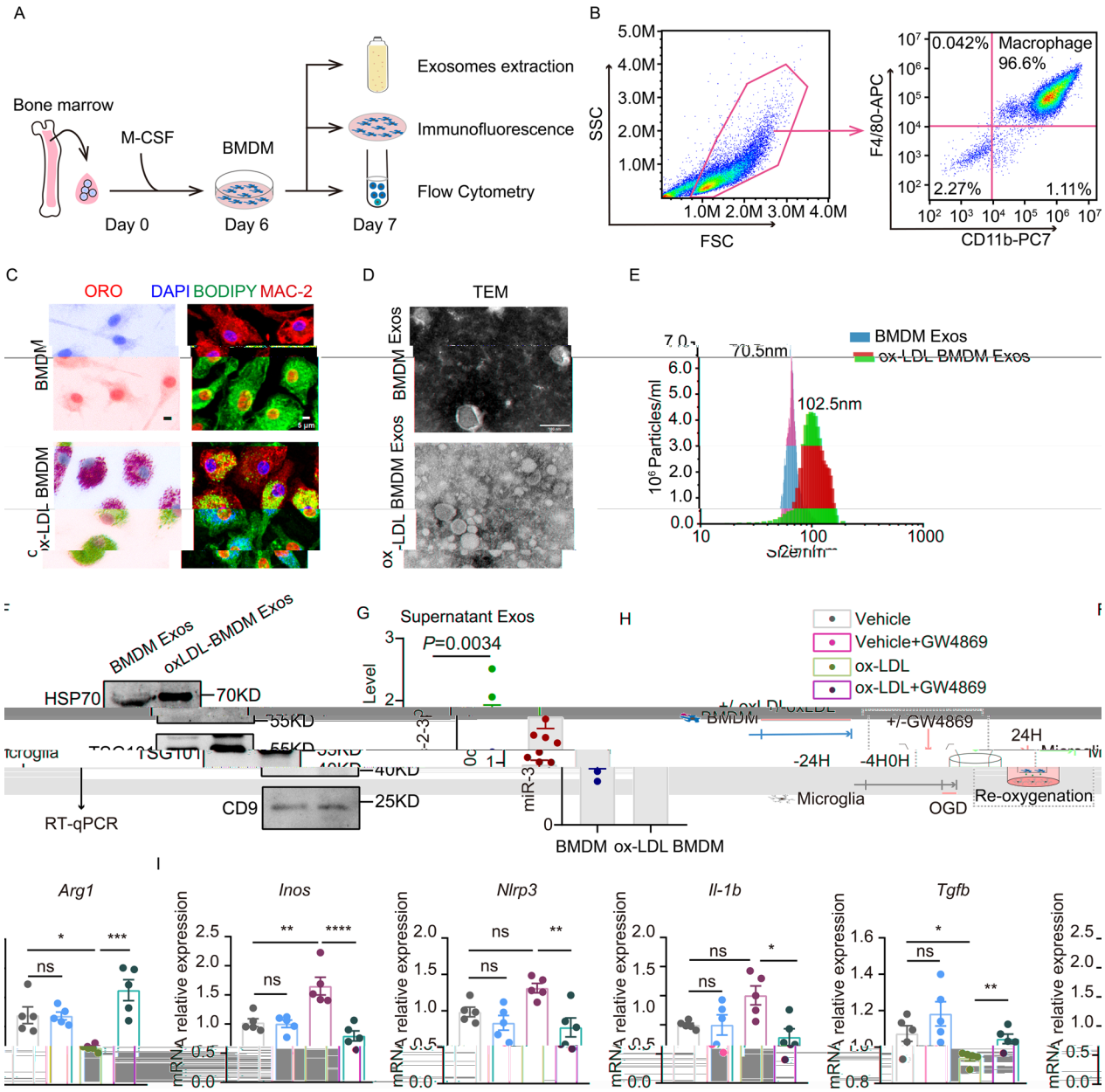

Fig. 4 Ox-LDL treated BMDM regulated inflammatory phenotype of microglia by secreting exosomal miR-30c-2-3p. **A** Schematic depicting culture of bone marrow derived macrophage for functional analysis. **B** Flow cytometry analysis of BMDM cells over 95% of the cells were positive for CD11b and F4/80. **C** Representative images of BMDMs and ox-LDL treated BMDMs stained with ORO and immunostained by MAC-2 and Bodipy. Scale bar, 5 μm. **D** Representative images of transmission electron microscope for exosomes from supernatant. Scale bar, 100 nm. **E** Diameter distribution of exosomes detecting by NTA. **F** Representative images of western blot for exosomal protein markers (HSP70, TSG101, CD9). **G** Relative supernatant exosomal miR-30c-2-3p level in ox-LDL treated BMDM group increased compared with BMDM group. n = 6 for each group. **H** Schematic depicting OGD pretreated microglia cocultured with BMDMs or ox-LDL pretreated BMDMs treated with or without GW4869. **I** Relative expression of the pro-inflammatory and anti-inflammatory genes in microglia cocultured with BMDMs or ox-LDL pretreated BMDMs treated with or without GW4869. n = 5 every group. Using One Way ANOVA test, $^{*}P < 0.05$, $^{**}P < 0.01$, $^{***}P < 0.001$, $^{****}P < 0.0001$

could be targeted directly by miR-30c-2-3p and the target position was AUUAGC (Fig. 5E).

Subsequently, to clarify the role of SMAD2 in microglial inflammatory polarization and the mechanism of miR-30c-2-3p affecting on microglia, si-Smad2 RNAs were transfected in microglia to knock down *Smad2* and miR-30c-2-3p mimics were transfected into microglia to overexpress miR-30c-2-3p (Fig. 6A). Compared

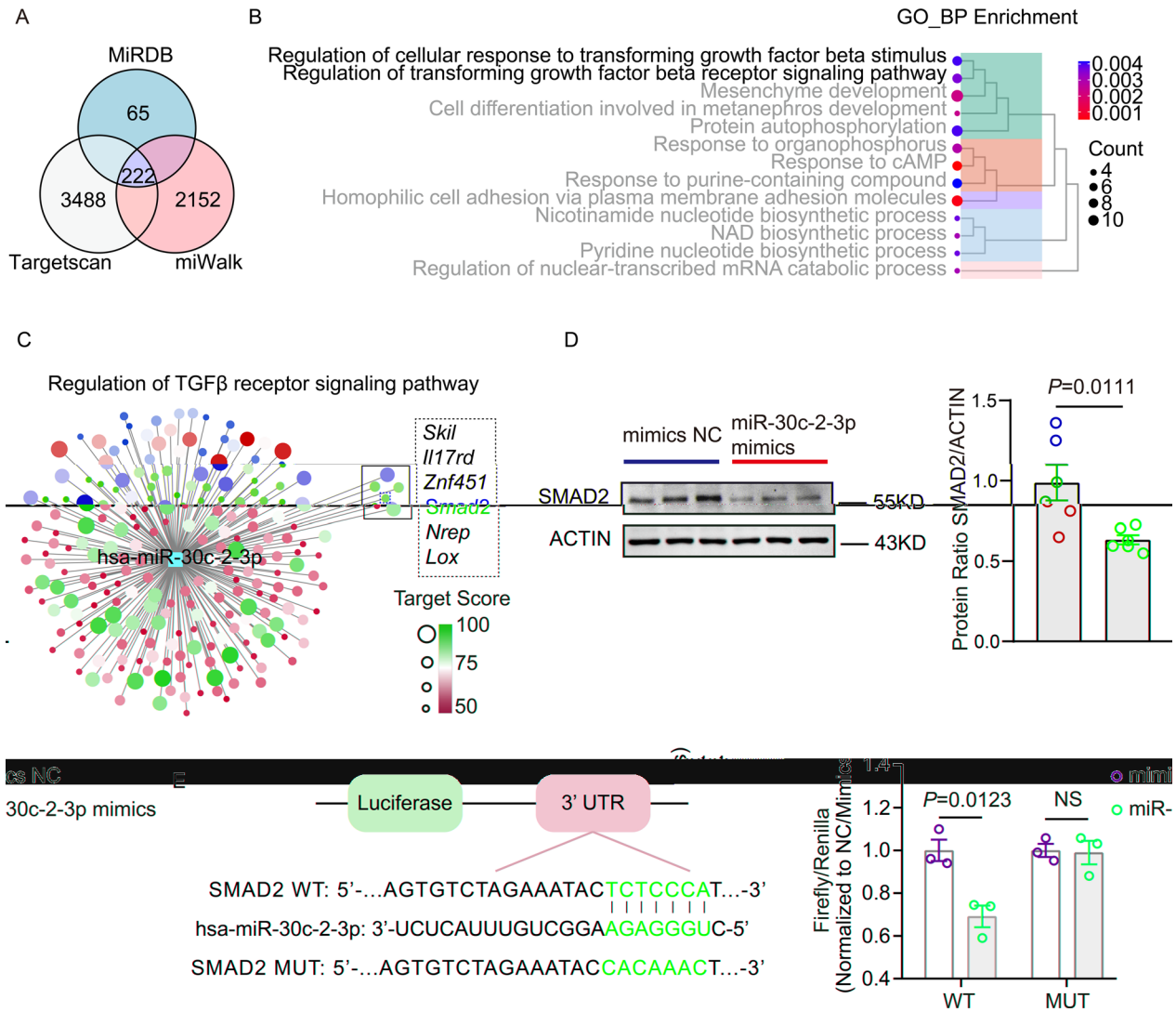

Fig. 5 MiR-30c-2-3p targeted *Smad2* involving in TGF-β receptor signaling pathway in microglia. **A** Venn diagrams showing miR-30c-2-3p predicted target relative uniqueness and overlap mRNA among data sets from MiRDB, Targetscan and miWalk. **B** GO functional enrichment analysis of the predicted target genes of miR-30c-2-3p, the color of each bubble represents the P value, and bubble size the gene number. **C** MiR-30c-2-3p targeted genes in the TGF-β signaling pathway (*Skil, Il17rd, Znf451, Smad2, Nrep, Lox*); the size and color of each bubble represents the Target Score. **D** Western blotting images and quantification for validation of the predicted target gene *Smad2*, n = 6 per group. **E** *Smad2* 3'UTR predicted regions targeted by miR-30c-2-3p in the left and dual luciferase reporter assay for clearing the combination between miR-30c-2-3p mimics and 3'UTR of *Smad2* (n = 3 per group)

to the siRNA NC group, the si-Smad2 group exhibited increased expression of pro-inflammatory genes *Il-6*, *Tnfa*, *Il-1b*, *Nlrp3*, but decreased expression of anti-inflammatory genes *Cd206*, *Tgfb*, *Arg1*, *Il-4* (Fig. 6B). Similarly, miR-30c-2-3p overexpression led to upregulation of those pro-inflammatory genes and downregulation of anti-inflammatory genes (Fig. 6B). Moreover, when si-Smad2 and miR-30c-2-3p mimics were co-transfected into microglia, pro-inflammatory changes were no longer observed (Supplemental Fig. 2C). Collectively, miR-30c-2-3p might regulate microglial neuroinflammation through inhibiting SMAD2. Additionally, the opposite regulation of inflammatory genes in microglia with miR-30c-2-3p mimics or inhibitor enhanced the pro-inflammation effects of miR-30c-2-3p (Supplemental Fig. 2B). Moreover, SMAD2 phosphorylation plays a key role in TGF-β signaling pathway. We next investigate changes in phosphorylation level of SMAD2. Results showed that total SMAD2 and p-SMAD2 protein level were both significantly decreased in microglia transfected with miR-30c-2-3p mimics or si-Smad2 after OGD

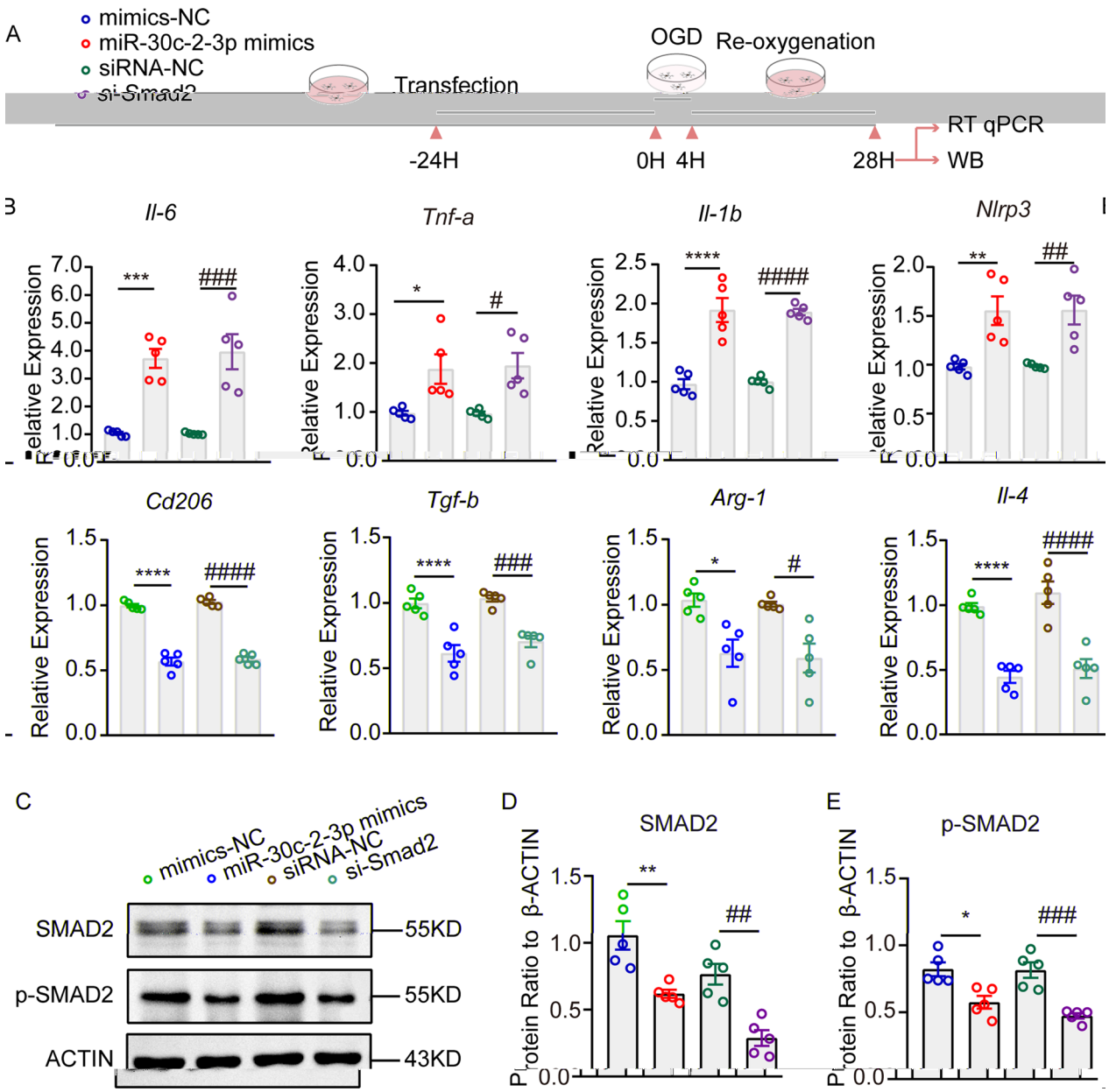

Fig. 6 MiR-30c-2-3p mimics transfection as well as si-Smad2 promoted microglia inflammation. **A** Schematic depicting for time point microglia transfected with mimics NC, miR-30c-2-3p mimics, siRNA NC, and siRNA Smad2, followed by OGD/R. **B** Relative expression of the pro-inflammatory and anti-inflammatory genes in microglia. Compared with mimics-NC group, $^{*}P<0.05$, $^{**}P<0.01$, $^{***}P<0.001$, $^{****}P<0.0001$; compared with siRNA-NC group, $^{\#}P<0.05$, $^{\#\#}P<0.01$, $^{\#\#\#}P<0.001$, $^{\#\#\#\#}P<0.0001$. **C**–**E** Western blotting images of SMAD2 and p-SMAD2 and protein expression analysis for microglia after transfecting. Compared with mimics-NC group, $^{*}P<0.05$, $^{**}P<0.01$, $^{***}P<0.001$, $^{****}P<0.0001$; compared with siRNA-NC group, $^{\#}P<0.05$, $^{\#\#}P<0.01$, $^{\#\#\#}P<0.001$, $^{\#\#\#\#}P<0.0001$

(Fig. 6C–E). Additionally, there was no change in the total SMAD2 and p-SMAD2 protein levels after transfecting microglia with si-Smad2 and miR-30c-2-3p mimics (Supplemental Fig. 2D). These data together revealed that miR-30c-2-3p might interfere with Smad2/TGF-β signaling pathway to promote pro-inflammatory phenotype of microglia.

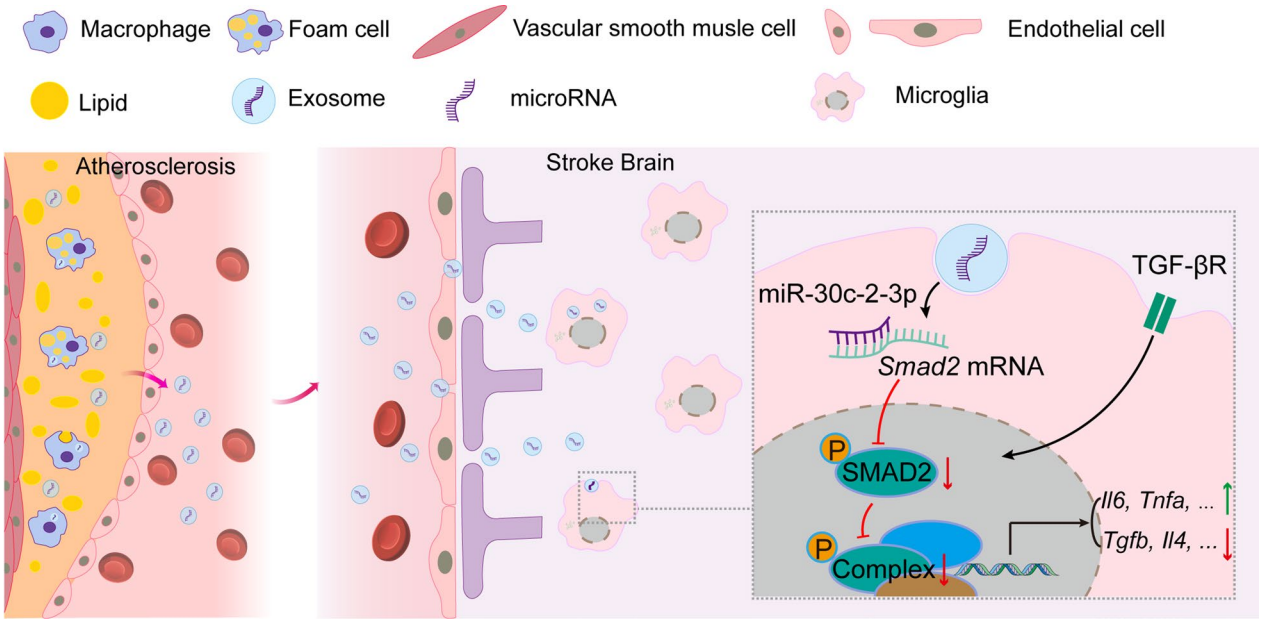

Fig. 7 The sketch map of the mechanism of exosomes-mediated ischemic stroke exacerbation. Exosomal miR-30c-2-3p, which originated predominantly from macrophage-derived foam cells, mainly targeted microglia to aggravate neuroinflammation during ischemic stroke

Discussion

This study demonstrated a potential mechanism that atherosclerosis exacerbate ischemic stroke through the remote transmission of the exosomal miR-30c-2-3p. Originating from macrophage-induced foam cells in atherosclerosis, exosomal miR-30c-2-3p targets Smad2 in microglia, aggravating neuroinflammation during ischemic stroke (Fig. 7).

With a focus on exosomes as biomarkers in AIS, we analyzed the potential of exosomal miR-30c-2-3p as a LAA subtype biomarker in plasma. Exosomes could exist for a relatively long time in the peripheral blood and various bioactive substances they carry can be stably detected [41]. During the development of AIS, significant alterations occur in the microRNA profile of circulating exosomes, suggesting possible application as emerging biomarkers for clinical diagnosis and prognostic assessment of acute ischemic stroke [42]. Previous studies have reported that brain-specific miR-9 and miR-124 were detected in serum exosomes of AIS patients with significantly higher expression levels than controls [43]. Our study revealed significantly higher expression levels of exosomal miR-30c-2-3p in AIS patients. Notably, while prior research has evaluated plasma microRNA profile in various diseases and identified upregulation of miR-30c-2-3p in coronary heart disease and other vascular disease [21–23], our findings suggested it potential as a biomarker specifically for AIS-LAA.

Increasing evidence supports the role of exosomes secreted by multiple cell types in atherosclerosis [13, 15, 17, 20, 44], and exosomes carrying various substances have been implicated in the progression of ischemic stroke [41, 45, 46]. However, studies on the exosomal mechanism of atherosclerosis participating in stroke are limited. Interestingly, our data demonstrated that atherosclerosis-derived exosomal miR-30c-2-3p influences the pathological niche during ischemic stroke. Furthermore, our findings indicate enrichment of exosomal miR-30c-2-3p derived from atherosclerotic foam cells. Foam cells are primarily generated by macrophages and smooth muscle cells [47], However, this study focused exclusively on macrophages, particularly in vitro.

ApoE$^{-/-}$ mice are widely used for constructing atherosclerosis model, with a high- fat diet leading to the formation of atherosclerotic plaques within 3 months [48]. Exosomes exhibit different characteristics depending on their sources or the physiological state of the body. Our experiments focused solely on the miR-30c-2-3p expression in ND or HFD exosomes. However, exosomes contain numerous bioactive substances, such as DNAs, proteins and metabolites, which can be detected by genomics for more clarity on their composition [49]. In the study, exosomes from atherosclerotic plaques were investigated the effects on stroke mice. However, *ApoE*$^{-/-}$ mice on high-fat diets rarely experience spontaneous stroke, as there usually require plaque rupture

[50]. *ApoE*$^{-/-}$ mice with tMCAO would exhibit increased neuroinflammation and exacerbated neurological impairment [51]. To avoid potential confounding factors related to APOE itself, this study did not conduct tMCAO in *ApoE*$^{-/-}$ mice.

Exosomes can be internalized by many recipient cells and release their contents to mediate cell communication [6]. Our study revealed that circulating AS exosomes predominantly enter microglia, where they stimulate microglia activation and provoke inflammatory responses. Microglia, serving as resident phagocytes in the central nervous system, became activated and engulf numerous substances, including necrotic cells or those crossing the damaged blood brain barrier [52–54]. Moreover, other cell types not addressed in this study, such as vascular smooth muscle cells that are part of the neurovascular unit, may also play a role. Exosomes could potentially influence the function of these vascular smooth muscle cells, leading to vasospasm. This vasospasm could, in turn, contribute to the promotion of stroke [55]. Previous study has shown that microglia internalized plasma EVs and adopt a pro-inflammatory phenotype [56]. MiRNAs, active substances in exosomes targeting recipient cells, may significantly influence gene expression by silencing specific mRNAs, thereby regulating protein bioactivity. Previous studies have showed that miR-30c-2-3p could target ATF1, TGF-β1 and RAB31 to inhibit these signaling pathways in different pathological states [26, 37, 57]. To elucidate the mechanism of exosomal miR-30c-2-3p affecting brain pathological microenvironment after ischemic stroke, in vitro experiments were conducted via co-culture system of macrophage and microglia. These experiments demonstrated that exosomal miR-30c-2-3p derived from macrophages-induced foam cells could directly promote microglial inflammation. The target genes of miR-30c-2-3p are enriched in TGF-β receptor signaling pathway with SMAD2 highly involved. A previous study showed that miR-30c-2-3p targeted TGF-β signaling pathway [58], which is associated with cell inflammation and apoptotic process. As the activation of TGF-β/Smad2/3 signaling pathway could promote anti-inflammatory responses of residing microglia within the ischemic cerebral environment [59], the inhibition of SMAD2 expression by miR-30c-2-3p is likely to induce a pro-inflammatory phenotype in microglia and subsequent neurological deficits. However, further studies of exploring the exact downstream molecules of SMAD2 were still warrant for confirming the molecular mechanism of TGFβ/SMAD2 in ischemic stroke due to LAA.

Several limitations should be considered in this study. Firstly, the exosomes isolated from atherosclerotic plaques might be contaminated by apoptotic bodies or proteins and could undergo enzyme damage during extraction, thereby altering their morphology [60]. Secondly, despite the fact that transmission electron microscopy, western blot, and nanoparticle tracking analysis (NTA) were conducted, it's still challenging to accurately distinguish exosomes from other extracellular vesicles with similar size. Thirdly, exosomes transport a variety of substances capable of influencing recipient cells, necessitating the detection of exosomal transcriptomics as a comprehensive approach [61]. Lastly, further studies are warranted to explore the dynamics of exosome procession and validate the involvement of TGF-β/SMAD2 signaling pathway in vivo.

Supplementary Information

The online version contains supplementary material available at https://doi.org/10.1186/s12974-024-03281-7.

Supplement Figure 1. The in vivo immunofluorescence and autofluorescence on the region of ischemic border. A, Representative images of immunostaining showed the region of ischemic border in stroke mouse brain and the distribution of Iba1^{+} cells. Scale bar of the left one, 200 μm; scale bar of the right three, 20 μm. B, Representative images of immunostaining showed there was almost no autofluorescence of lysosomes in stroke mouse brain. Scale bar, 20 μm.

Supplement Figure 2. MiR-30c-2-3p might promote microglial inflammatory properties by targeting SMAD2 pathway. A, Relative expression of the pro-inflammatory and anti-inflammatory genes in microglia with OGD/R treatment. *$P < 0.05$, **$P < 0.01$, ***$P < 0.001$, ****$P < 0.0001$. B, Relative expression of the pro-inflammatory and anti-inflammatory genes in microglia with OGD/R treatment transfected with Mimic-NC/MiR-30c-2-3p mimics/Inhibitor NC/MiR-30c-2-3p inhibitor. *$P < 0.05$, **$P < 0.01$, ***$P < 0.001$, ****$P < 0.0001$. C, Relative expression of the pro-inflammatory and anti-inflammatory genes in microglia with OGD/R and si-SMAD2 treatment transfected with MiR-30c-2-3p mimics or not. D, Western blotting images of SMAD2 and p-SMAD2 and protein expression analysis for microglia with OGD/R and si-SMAD2 treatment transfected with MiR-30c-2-3p mimics or not.

Supplementary Material 3

Acknowledgements

We thank Prof. Sheng Wang and Prof. Ru-Dong Chen (Department of Neurosurgery, Tongji Hospital) for providing carotid endarterectomy samples. In addition, we are greatly indebted to all the patients who participated in the study, without whom this study would never have been accomplished.

Author contributions

D.S.T., C.Q., W.W., Y.T., M.H.D. and L.Q.Z. conceptualized and designed the study. C.Q., M.H.D., Y.T., X.W.P., H.Z., Y.H.C., L.Q.Z. and S.Y. analyzed data. W.W., D.S.T., C.Q., M.H.D., L.Q.Z., L.Y.Z., Y.F.Y. and X.W.P. interpreted data. D.S.T., C.Q., Y.T., M.H.D, and L.F.Z. drafted the manuscript. W.W., D.S.T., C.Q., M.H.D., Y.T. , X.W.P., H.Z.,Y.H.C., L.Q.Z., S.Y., L.Y.Z., Y.F.Y.and L.F.Z. made critical revision of the manuscript. All authors were involved in collection, and critical review of the data. All authors approved the final version of the manuscript.

Funding

This study was funded by STI2030-Major Projects 2022ZD0204700 (WW), National Natural Science Foundation of China (grants 82371404, 82071380 to D.-S.T. and 82271341 to C.Q.), Hubei Province Key Research and Development Program Project (2023BCB148 to D.-S. T), Basic Research Support Program of Huazhong University of Science and Technology (2024BRB023 to C.Q.) and Knowledge Innovation Program of Wuhan Shuguang Project (2022020801020454 to C.Q.).

Availability of data and materials
All the data and methods supporting the findings of the study are available from the corresponding authors upon reasonable request.

Declarations

Ethics approval and consent to participate
The study was approved by the Ethics Committee of Tongji Hospital and eligible subjects gave informed signed consent.

Competing interests
The authors declare no competing interests.

Received: 4 May 2024 Accepted: 29 October 2024
Published online: 08 November 2024

References

1. Feigin VL, Brainin M, Norrving B, Martins S, Sacco RL, Hacke W, et al. World Stroke Organization (WSO): global stroke fact sheet 2022. Int J Stroke. 2022;17(1):18–29.
2. Holmstedt CA, Turan TN, Chimowitz MI. Atherosclerotic intracranial arterial stenosis: risk factors, diagnosis, and treatment. Lancet Neurol. 2013;12(11):1106–14.
3. Goldstein LB. Acute ischemic stroke treatment in 2007. Circulation. 2007;116(13):1504–14.
4. Qin C, Yang S, Chu YH, Zhang H, Pang XW, Chen L, et al. Signaling pathways involved in ischemic stroke: molecular mechanisms and therapeutic interventions. Signal Transduct Target Ther. 2022;7(1):215.
5. Buzas EI. The roles of extracellular vesicles in the immune system. Nat Rev Immunol. 2022;23:236.
6. Kalluri R, LeBleu VS. The biology, function, and biomedical applications of exosomes. Science. 2020;367:6478.
7. van Niel G, D'Angelo G, Raposo G. Shedding light on the cell biology of extracellular vesicles. Nat Rev Mol Cell Biol. 2018;19(4):213–28.
8. Andaloussi SEL, Mäger I, Breakefield XO, Wood MJ. Extracellular vesicles: biology and emerging therapeutic opportunities. Nat Rev Drug Discov. 2013;12(5):347–57.
9. Zhang T, Ma S, Lv J, Wang X, Afewerky HK, Li H, et al. The emerging role of exosomes in Alzheimer's disease. Ageing Res Rev. 2021;68: 101321.
10. Wang X, Zhou Y, Gao Q, Ping D, Wang Y, Wu W, et al. The role of exosomal microRNAs and oxidative stress in neurodegenerative diseases. Oxid Med Cell Longev. 2020;2020:3232869.
11. Guo M, Wang J, Zhao Y, Feng Y, Han S, Dong Q, et al. Microglial exosomes facilitate α-synuclein transmission in Parkinson's disease. Brain. 2020;143(5):1476–97.
12. Wang C, Li Z, Liu Y, Yuan L. Exosomes in atherosclerosis: performers, bystanders, biomarkers, and therapeutic targets. Theranostics. 2021;11(8):3996–4010.
13. Bouchareychas L, Duong P, Covarrubias S, Alsop E, Phu TA, Chung A, et al. Macrophage exosomes resolve atherosclerosis by regulating hematopoiesis and inflammation via MicroRNA Cargo. Cell Rep. 2020;32(2): 107881.
14. Zhu J, Liu B, Wang Z, Wang D, Ni H, Zhang L, et al. Exosomes from nicotine-stimulated macrophages accelerate atherosclerosis through miR-21-3p/PTEN-mediated VSMC migration and proliferation. Theranostics. 2019;9(23):6901–19.
15. Niu C, Wang X, Zhao M, Cai T, Liu P, Li J, et al. Macrophage foam cell-derived extracellular vesicles promote vascular smooth muscle cell migration and adhesion. J Am Heart Assoc. 2016;5(10):e004099.
16. Christersson C, Thulin Å, Siegbahn A. Microparticles during long-term follow-up after acute myocardial infarction. Association to atherosclerotic burden and risk of cardiovascular events. Thromb Haemost. 2017;117(8):1571–81.
17. Nguyen MA, Karunakaran D, Geoffrion M, Cheng HS, Tandoc K, Perisic Matic L, et al. Extracellular vesicles secreted by atherogenic macrophages transfer MicroRNA to inhibit cell migration. Arterioscler Thromb Vasc Biol. 2018;38(1):49–63.
18. Paone S, Baxter AA, Hulett MD, Poon IKH. Endothelial cell apoptosis and the role of endothelial cell-derived extracellular vesicles in the progression of atherosclerosis. Cell Mol Life Sci. 2019;76(6):1093–106.
19. McDonald MK, Tian Y, Qureshi RA, Gormley M, Ertel A, Gao R, et al. Functional significance of macrophage-derived exosomes in inflammation and pain. Pain. 2014;155(8):1527–39.
20. Peng M, Sun R, Hong Y, Wang J, Xie Y, Zhang X, et al. Extracellular vesicles carrying proinflammatory factors may spread atherosclerosis to remote locations. Cell Mol Life Sci. 2022;79(8):430.
21. Zhou ZM, Chen J, Wu TS, Liu QC, Song HW, Sun SC. Profiling of plasma circulating miRNA in coronary heart disease patients detected by next-generation small RNA sequencing. Int J Clin Exp Med. 2017;10(5):8060–8.
22. Zhang T, Tian F, Wang J, Jing J, Zhou SS, Chen YD. Endothelial cell autophagy in atherosclerosis is regulated by miR-30-mediated translational control of ATG6. Cell Physiol Biochem. 2015;37(4):1369–78.
23. Hu F, Liu H, Wang C, Li H, Qiao L. Expression of the microRNA-30 family in pulmonary arterial hypertension and the role of microRNA-30d-5p in the regulation of pulmonary arterial smooth muscle cell toxicity and apoptosis. Exp Ther Med. 2022;23(1):108.
24. Xie S, Niu W, Xu F, Wang Y, Hu S, Niu C. Differential expression and significance of miRNAs in plasma extracellular vesicles of patients with Parkinson's disease. Int J Neurosci. 2022;132(7):673–88.
25. Huang Y, Liu Z, Li N, Tian C, Yang H, Huo Y, et al. Parkinson's disease derived exosomes aggravate neuropathology in SNCA*A53T mice. Ann Neurol. 2022;92(2):230–45.
26. Tang CT, Liang Q, Yang L, Lin XL, Wu S, Chen Y, et al. RAB31 targeted by MiR-30c-2-3p regulates the GLI1 signaling pathway, affecting gastric cancer cell proliferation and apoptosis. Front Oncol. 2018;8:554.
27. Moch H, Lukamowicz-Rajska M. miR-30c-2-3p and miR-30a-3p: new pieces of the jigsaw puzzle in HIF2α regulation. Cancer Discov. 2014;4(1):22–4.
28. Lovett JK, Gallagher PJ, Hands LJ, Walton J, Rothwell PM. Histological correlates of carotid plaque surface morphology on lumen contrast imaging. Circulation. 2004;110(15):2190–7.
29. Virmani R, Kolodgie FD, Burke AP, Farb A, Schwartz SM. Lessons from sudden coronary death: a comprehensive morphological classification scheme for atherosclerotic lesions. Arterioscler Thromb Vasc Biol. 2000;20(5):1262–75.
30. Cai G, Cai G, Zhou H, Zhuang Z, Liu K, Pei S, et al. Mesenchymal stem cell-derived exosome miR-542-3p suppresses inflammation and prevents cerebral infarction. Stem Cell Res Ther. 2021;12(1):2.
31. Tian T, Zhang HX, He CP, Fan S, Zhu YL, Qi C, et al. Surface functionalized exosomes as targeted drug delivery vehicles for cerebral ischemia therapy. Biomaterials. 2018;150:137–49.
32. Luo L, Liu M, Fan Y, Zhang J, Liu L, Li Y, et al. Intermittent theta-burst stimulation improves motor function by inhibiting neuronal pyroptosis and regulating microglial polarization via TLR4/NFκB/NLRP3 signaling pathway in cerebral ischemic mice. J Neuroinflammation. 2022;19(1):141.
33. Zhou L-Q, Dong M-H, Hu Z-W, Tang Y, Chu Y-H, Chen M, et al. Staged suppression of microglial autophagy facilitates regeneration in CNS demyelination by enhancing the production of linoleic acid. Proc Natl Acad Sci. 2023;120(1): e2209990120.
34. Yang S, Qin C, Chen M, Chu YH, Tang Y, Zhou LQ, et al. TREM2-IGF1 mediated glucometabolic enhancement underlies microglial neuroprotective properties during ischemic stroke. Adv Sci (Weinh). 2024;11(10): e2305614.
35. Laigle V, Dingli F, Amhaz S, Perron T, Chouchène M, Colasse S, et al. Quantitative ubiquitylome analysis reveals the specificity of RNF111/Arkadia E3 ubiquitin ligase for its degradative substrates SKI and SKIL/SnoN in TGF-β signaling pathway. Mol Cell Proteomics. 2021;20: 100173.
36. Zhang Y, Wang W, Min J, Liu S, Wang Q, Wang Y, et al. ZNF451 favors triple-negative breast cancer progression by enhancing SLUG-mediated CCL5 transcriptional expression. Cell Rep. 2023;42(6): 112654.
37. Li Z, Shi L, Li X, Wang X, Wang H, Liu Y. RNF144A-AS1, a TGF-β1- and hypoxia-inducible gene that promotes tumor metastasis and proliferation via targeting the miR-30c-2-3p/LOX axis in gastric cancer. Cell Biosci. 2021;11(1):177.
38. Liu S, Fu Y, Mei K, Jiang Y, Sun X, Wang Y, et al. A shedding soluble form of interleukin-17 receptor D exacerbates collagen-induced arthritis through facilitating TNF-α-dependent receptor clustering. Cell Mol Immunol. 2021;18(8):1883–95.

39. De Jesus DF, Orime K, Kaminska D, Kimura T, Basile G, Wang CH, et al. Parental metabolic syndrome epigenetically reprograms offspring hepatic lipid metabolism in mice. J Clin Invest. 2020;130(5):2391–407.
40. Abdel Mouti M, Pauklin S. TGFB1/INHBA homodimer/nodal-SMAD2/3 signaling network: a pivotal molecular target in PDAC treatment. Mol Ther. 2021;29(3):920–36.
41. Xu Y, Hu Y, Xu S, Liu F, Gao Y. Exosomal microRNAs as potential biomarkers and therapeutic agents for acute ischemic stroke: new expectations. Front Neurol. 2021;12: 747380.
42. Forró T, Bajkó Z, Bălașa A, Bălașa R. Dysfunction of the neurovascular unit in ischemic stroke: highlights on microRNAs and exosomes as potential biomarkers and therapy. Int J Mol Sci. 2021;22(11):5621.
43. Ji Q, Ji Y, Peng J, Zhou X, Chen X, Zhao H, et al. Increased brain-specific MiR-9 and MiR-124 in the serum exosomes of acute ischemic stroke patients. PLoS ONE. 2016;11(9): e0163645.
44. Wang C, Liu C, Shi J, Li H, Jiang S, Zhao P, et al. Nicotine exacerbates endothelial dysfunction and drives atherosclerosis via extracellular vesicle-miRNA. Cardiovasc Res. 2022;119:729.
45. Liu Y, Li Y, Zang J, Zhang T, Li Y, Tan Z, et al. CircOGDH is a penumbra biomarker and therapeutic target in acute ischemic stroke. Circ Res. 2022;130(6):907–24.
46. Yang L, Han B, Zhang Z, Wang S, Bai Y, Zhang Y, et al. Extracellular vesicle-mediated delivery of circular RNA SCMH1 promotes functional recovery in rodent and nonhuman primate ischemic stroke models. Circulation. 2020;142(6):556–74.
47. Li Y, Zhu H, Zhang Q, Han X, Zhang Z, Shen L, et al. Smooth muscle-derived macrophage-like cells contribute to multiple cell lineages in the atherosclerotic plaque. Cell Discov. 2021;7(1):111.
48. Emini Veseli B, Perrotta P, De Meyer GRA, Roth L, Van der Donckt C, Martinet W, et al. Animal models of atherosclerosis. Eur J Pharmacol. 2017;816:3–13.
49. Jeppesen DK, Fenix AM, Franklin JL, Higginbotham JN, Zhang Q, Zimmerman LJ, et al. Reassessment of exosome composition. Cell. 2019;177(2):428–45.
50. Van der Donckt C, Van Herck JL, Schrijvers DM, Vanhoutte G, Verhoye M, Blockx I, et al. Elastin fragmentation in atherosclerotic mice leads to intraplaque neovascularization, plaque rupture, myocardial infarction, stroke, and sudden death. Eur Heart J. 2015;36(17):1049–58.
51. Leng C, Lin K, Zhou M, Tao X, Sun B, Shu X, et al. Apolipoprotein E deficiency exacerbates blood–brain barrier disruption and hyperglycemia-associated hemorrhagic transformation after ischemic stroke. J Stroke Cerebrovasc Dis. 2024;33(11): 107987.
52. Chen M, Zhang H, Chu YH, Tang Y, Pang XW, Qin C, et al. Microglial autophagy in cerebrovascular diseases. Front Aging Neurosci. 2022;14:1023679.
53. Fu R, Shen Q, Xu P, Luo JJ, Tang Y. Phagocytosis of microglia in the central nervous system diseases. Mol Neurobiol. 2014;49(3):1422–34.
54. Hu X, Li P, Guo Y, Wang H, Leak RK, Chen S, et al. Microglia/macrophage polarization dynamics reveal novel mechanism of injury expansion after focal cerebral ischemia. Stroke. 2012;43(11):3063–70.
55. Kaufmann J, Buecke P, Meinel T, Beyeler M, Scutelnic A, Kaesmacher J, et al. Frequency of ischaemic stroke and intracranial haemorrhage in patients with reversible cerebral vasoconstriction syndrome (RCVS) and posterior reversible encephalopathy syndrome (PRES)—a systematic review. Eur J Neurol. 2024;31(5): e16246.
56. Zhang H, Lin S, McElroy CL, Wang B, Jin D, Uteshev VV, et al. Circulating pro-inflammatory exosomes worsen stroke outcomes in aging. Circ Res. 2021;129(7):e121–40.
57. Nguyen HT, Jia W, Beedle AM, Kennedy EJ, Murph MM. Lysophosphatidic acid mediates activating transcription factor 3 expression which is a target for post-transcriptional silencing by miR-30c-2-3p. PLoS ONE. 2015;10(9): e0139489.
58. Fang L, Wu S, Zhu X, Cai J, Wu J, He Z, et al. MYEOV functions as an amplified competing endogenous RNA in promoting metastasis by activating TGF-β pathway in NSCLC. Oncogene. 2019;38(6):896–912.
59. Zhang L, Wei W, Ai X, Kilic E, Hermann DM, Venkataramani V, et al. Extracellular vesicles from hypoxia-preconditioned microglia promote angiogenesis and repress apoptosis in stroke mice via the TGF-β/Smad2/3 pathway. Cell Death Dis. 2021;12(11):1068.
60. Vella LJ, Scicluna BJ, Cheng L, Bawden EG, Masters CL, Ang CS, et al. A rigorous method to enrich for exosomes from brain tissue. J Extracell Vesicles. 2017;6(1):1348885.
61. Crescitelli R, Lasser C, Jang SC, Cvjetkovic A, Malmhall C, Karimi N, et al. Subpopulations of extracellular vesicles from human metastatic melanoma tissue identified by quantitative proteomics after optimized isolation. J Extracell Vesicles. 2020;9(1):1722433.

Publisher's Note